HHS Public Access

Author manuscript

Cancer Cell. Author manuscript; available in PMC 2019 December 10.

Published in final edited form as:

Cancer Cell. 2018 December 10; 34(6): 893–905.e8. doi:10.1016/j.ccell.2018.11.006.

Loss of the FAT1 tumor suppressor promotes resistance to CDK4/6 inhibitors via the Hippo pathway

Zhiqiang Li[#1], **Pedram Razavi**[#1,2,3], **Qing Li**[#1], **Weiyi Toy**[1], **Bo Liu**[1], **Christina Ping**[2], **Wilson Hsieh**[1], **Francisco Sanchez-Vega**[1], **David N. Brown**[4], **Arnaud F. Da Cruz Paula**[4], **Luc Morris**[1], **Pier Selenica**[3], **Emily Eichenberger**[3], **Ronglai Shen**[5], **Nikolaus Schultz**[1], **Neal Rosen**[2,3], **Maurizio Scaltriti**[1,4], **Edi Brogi**[4], **Jose Baselga**[1,2,*], **Jorge S. Reis-Filho**[4], and **Sarat Chandarlapaty**[1,2,3,7,**]

[1]Human Oncology and Pathogenesis Program, Memorial Sloan Kettering Cancer Center (MSKCC), New York, NY 10065, USA

[2]Breast Medicine Service, Department of Medicine, MSKCC, New York, NY 10065, USA

[3]Weill-Cornell Medical College, New York, NY 10065, USA

[4]Department of Pathology, MSKCC, New York, NY 10065, USA

[5]Department of Epidemiology and Biostatistics, MSKCC, New York, NY 10065, USA

[7]Lead Contact

[*]Current affiliation, Vall d'Hebron Institute of Oncology, Barcelona, Spain

[#] These authors contributed equally to this work.

SUMMARY

CDK4/6 inhibitors (CDK4/6i) are effective in breast cancer, however drug resistance is frequently encountered and poorly understood. We conducted a genomic analysis of 348 estrogen receptor-positive breast cancers treated with CDK4/6i and identified loss of function mutations affecting

[**]Correspondence: chandars@mskcc.org.

AUTHOR CONTRIBUTIONS

S.C., P.R., Z.L., Q.L. designed the study. S.C., Z.L., P.R., Q.L., W.T., C.Y., B.L., C.P., E.E., F.SV., N.S., D.B. E.B., P.S., A.F.D-C-P., R.S., and J.S.R-F. generated and analyzed the data. S.C., Z.L., P.R., Q.L., W.T., B.L., C.P., C.Y., F.S-V, P.S., N.S., N.R., M.S., R.S., J.B., and J.S.R-F wrote the manuscript.

DECLARATION OF INTERESTS

P.R. has received consulting fees from Novartis. L.M. was previously on an advisory board for Merck. N.R. is on the SABs of Astra-Zeneca, Beigene, Chugai, Daichi-Sankyo, Fprime and Fortress and was on the SAB of Araxes, Kura, Takeda, Tarveda and Kadmon. He has consulted for Novartis, Array and Boeringher-Mannheim. He has equity in in Beigne, Kura, Araxes and Zai Labs. He receives research grants from Chugai. M.S. received research funds from Puma Biotechnology, Daiichi-Sankyo, and Menarini Ricerche and is a cofounder of Medendi Medical Travel. J.B. has received honoraria from Roche, Lilly, and Novartis; served on the board of directors for Varian Medical Systems, Bristol-Myers Squibb, and Foghorn; is a past board member of Grail, Aura Biosciences, and Infinity Pharmaceuticals; is on the scientific advisory boards of Grail, PMV Pharma, ApoGen, Juno, Roche, Lilly, Novartis, Northern Biologicals, and Tango Therapeutics; is a founder of Venthera; and has stock or other ownership interests in PMV Pharma, Grail, Varian, Foghorn, Aura, Infinity, and ApoGen, as well Tango and Venthera. J.S.R-F is on scientific advisory boards of Paige.AI and Volition Rx and received consulting fees from Goldman Sachs. S.C. has received research funds in the past from Novartis and Eli Lilly and ad hoc consulting honoraria from Novartis, Sermonix, Context Therapeutics, and Revolution Medicines.

FAT1 and *RB1* linked to drug resistance. FAT1 loss led to marked elevations in CDK6 whose suppression restored sensitivity to CDK4/6i. The induction of CDK6 was mediated by the Hippo pathway with accumulation of YAP and TAZ transcription factors on the *CDK6* promoter. Genomic alterations in other Hippo pathway components were also found to promote CDK4/6i resistance. These findings uncover a tumor suppressor function of Hippo signaling in ER^+ breast cancer and establish FAT1 loss as a mechanism of resistance to CDK4/6i.

Graphical Abstract

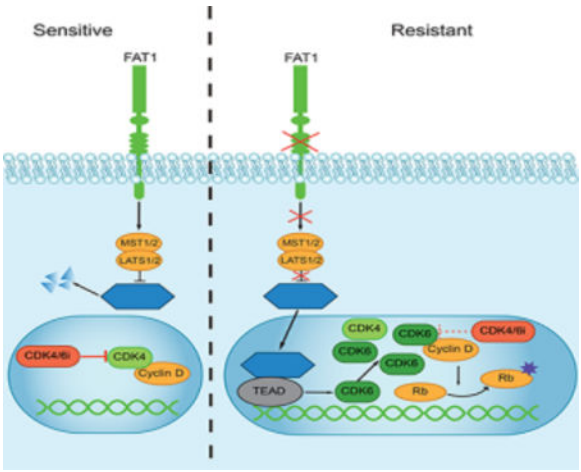

Keywords

CDK4/6 inhibitors; Palbociclib; Ribociclib; Abemaciclib; Hippo pathway; Breast cancer; Drug resistance; FAT1; YAP; RB1

INTRODUCTION

Estrogen driven activation of cyclin D-CDK4/6 kinase is essential for physiologic mammary development and proliferation of estrogen receptor-positive (ER^+) breast cancers. Multiple clinical trials have established the efficacy of ATP competitive CDK4/6 kinase inhibitors (CDK4/6i) palbociclib (Finn et al., 2016; Turner et al., 2015), ribociclib (Hortobagyi et al., 2016) and abemaciclib (Dickler et al., 2017; Sledge et al., 2017) in the treatment of advanced ER^+ breast cancer. Despite the substantial improvements in activity afforded by these drugs, some tumors never respond and most patients ultimately experience disease progression. Several studies have uncovered the biologic basis for resistance to antiestrogen therapy involving restored cyclin D-CDK4/6 activity such as through activating mutations in *ESR1* (Jeselsohn et al., 2014; Robinson et al., 2013; Toy et al., 2013) or *ERBB2* amplification (Johnston et al., 2009). However, the molecular basis for drug resistance to CDK4/6i is unknown and represents a pressing medical need as most patients with metastatic ER^+ breast cancer (MBC) are now receiving this drug as front-line therapy. In this study, we sought to identify whether any recurrent genomic alterations are associated with poor response to CDK4/6i and functionally characterize how such alterations modify cyclin D-CDK4/6-mediated growth control.

RESULTS

FAT1 loss is associated with poor outcome on CDK4/6 inhibitor therapy

To establish whether any genetic alterations might be associated with resistance to CDK4/6i in patients, we subjected 348 $ER^+/HER2^-$ breast cancers to targeted sequencing of >340 cancer associated genes (MSK-IMPACT) (Razavi et al., 2018; Zehir et al., 2017) (Tables S1, S2). These tumors were procured prior to initiation of any of the three clinically efficacious CDK4/6i (palbociclib, ribociclib or abemaciclib; although the majority of patients received palbociclib in this cohort). Analysis of somatic mutations and copy number alterations (Figure S1) inferred to be biologically and therapeutically relevant (Chakravarty et al., 2017; Chang et al., 2016; Razavi et al., 2018) (Table S3) revealed that common alterations such as *CCND1* amplification, *PIK3CA* mutations, and *ESR1* mutations had no association with progression-free survival (PFS) on the drug (Figure 1A-C, Table S4), consistent with prior reports (Finn et al., 2015; Turner et al., 2015). In a small group of patients with tumors harboring alterations resulting in loss of the *FAT1* or *RB1*, however, PFS was drastically shorter (Figure 1A, Table S4). Whereas the association of *RB1* loss with CDK4/6i resistance (median PFS of 3.6 months, 95% CI: 2.2, not reached, log-rank p value = 0.00041, Figure 1D) was anticipated (DeCaprio et al., 1989; Fry et al., 2004; Matsushime et al., 1992) based on the mechanism of drug action, the link between *FAT1* loss and drug resistance was not.

FAT1 loss promotes CDK4/6i resistance

FAT1 has been previously linked to cancer cell growth with loss of function mutations linked to progression of head and neck cancer (Morris et al., 2013). Across 1501 $ER^+/HER2^-$ breast cancers sequenced at MSKCC (Razavi et al., 2018), mutations in *FAT1* are observed in ~2% of primary and ~6% of metastatic tumors (Figure 2A). Recurrent, hotspot mutations were not identified in this series, however, deleterious mutations (truncating, frameshifting, and splice site mutations, or homozygous deletion) comprised roughly 1/3 of the genomic alterations. The concurrent alterations present in *FAT1* mutated tumors appear qualitatively similar to those found in other $ER^+/HER2^-$ breast cancers with frequent mutations in *PIK3CA* and *TP53* (Figure 2B). Among the patients with a deleterious *FAT1* mutation in their tumor who received CDK4/6i therapy, the median PFS was 2.4 months (95% confidence interval [CI]: 2.0, not reached) versus 10.1 months (95% CI: 8.7, 12.2) for unaffected patients (log-rank p value = $2.2x10^{-11}$, Figure 2C). This effect was found to be like that observed with *RB1* loss of function mutations or homozygous deletion. We confirmed our findings by utilizing a different method for the identification of somatic mutations most likely to be deleterious (Martelotto et al., 2014; Yates et al., 2017) (STAR Methods) and once again, alterations in both *FAT1* and *RB1* were found to be significantly associated with poor response (Table S3). Additionally, after adjustment for the tumor mutational burden (TMB) per sample or the number of previous lines of therapy in metastatic setting, alterations resulting in loss of *FAT1* and *RB1* remained significant (Table S3). Consistent with the role of a *bona fide* tumor suppressor gene (Polak et al., 2017; Riaz et al., 2017), the effect of *FAT1* alterations on CDK4/6i sensitivity was most apparent in those cases with bi-allelic *FAT1* inactivation (pathogenic mutation coupled with loss of the wild-type allele, dual pathogenic mutations, or homozygous deletion), whereas only a subset of patients with missense mutations had short PFS (Figure 2C).

Finally, we assessed the treatment history of patients with *FAT1* alterations in the total cohort of $ER^+/HER2^-$ breast cancer patients (Figure 2B) including those who previously received a CDK4/6i. We identified a patient with metastatic $ER^+/HER2^-$ breast cancer who received palbociclib and fulvestrant and had a mixed response on her first scan. The patient's liver lesions progressed rapidly (PFS of 2.5 months, Figure 2D) but her tumors in the lung and thoracic lymph nodes responded to therapy. A deleterious structural rearrangement in chromosome 4 resulting in the fusion of *ADAM29* and *FAT1*, and deletion of the majority of *FAT1* exonic and intronic regions, was identified in a post-treatment biopsy of the progressing liver metastasis (Figure 2E-2F). The allele-specific copy number analysis of this specimen identified loss of heterozygosity of *FAT1* (Figure S2A), indicating that this deleterious rearrangement likely resulted in a complete loss of function of *FAT1*. The patient also had a pre-treatment biopsy of a metastatic lung tumor, which responded to CDK4/6i. In comparing the two samples, the *ADAM29-FAT1* fusion was the only alteration that was called in the post-treatment liver tumor and not in the pre-treatment lung tumor (Figure 2E and S2B) further associating *FAT1* loss of function alteration with resistance to therapy. Taken together, these genomic data strongly link loss of function mutations in the *FAT1* and *RB1* tumor suppressors as mediators of resistance to CDK4/6i.

FAT1 loss leads to resistance to CDK4/6 inhibitors

To establish whether and how *FAT1* loss might mediate CDK4/6i resistance, we engineered multiple *FAT1* knockout (99% protein suppression) and knockdown (85–95% protein suppression) cell lines from the ER^+, CDK4/6i sensitive MCF7 model (Figure S3A). Loss of FAT1 expression was not associated with accelerated growth of tumor cells under drug-free conditions (Figure 3A). Upon exposure to 50 nM abemaciclib (LY2835219), however, growth of parental MCF7 cells was completely inhibited whereas MCF7 cells with *FAT1* knockout or knockdown were not (Figure 3B, Figure S3B). To determine whether drug resistance might be through an insensitive CDK4/6 kinase activity, we assessed phosphorylation of CDK4/6 substrate after 24 hours of drug exposure (Figure 3C). Whilst Rb phosphorylation (S780, S807, S811) was completely blocked by drug in parental MCF7 cells, there was only partial inhibition in the FAT1 suppressed cells. These data are consistent with the observation that *FAT1* loss did not completely eliminate the effect of the drug, but rather increased the growth inhibitory concentration (IC_{50}) on the order of 4–6 folds, comparable to the effect of Rb loss and enforced CDK6 overexpression (Figure 3D, Figure S3C, D).

We next sought to confirm that these effects were not restricted to the incipient cell line model or particular CDK4/6i used in these experiments. We examined the impact of *FAT1* knockout or knockdown on the CDK4/6i sensitive ER^+ CAMA-1 cell line and again found that loss of FAT1 was associated with a diminished response to abemaciclib (Figure S3E). We further tested the effect of the other FDA approved CDK4/6i (palbociclib and ribociclib) and observed that FAT1 suppressed cells consistently require higher doses of drug to fully inhibit Rb phosphorylation and block proliferation (Figure 3D, Figure S3F).

FAT1 loss induces the expression of CDK6

As *FAT1* loss led to a change in the concentration at which chemically distinct CDK4/6i could block Rb phosphorylation, we posited that components of the cyclinD-CDK4/6 complex may be subject to FAT1 regulation. We examined mRNA and protein levels of these components and noted a striking increase of CDK6 levels in all FAT1 suppressed models (Figure 4A, B). The induction of CDK6 was not restricted to the MCF7-FAT1 suppressed models as we also observed upregulation of CDK6 in the CAMA-1 FAT1 suppressed models as well (Figure 4C). This is consistent with data from The Cancer Genome Atlas (TCGA) showing significantly higher levels of CDK6 transcripts in *FAT1*-deleted samples than those in *FAT1* wild-type samples in ER^+ breast cancers (Figure 4D). We further noted that basal levels of CDK6 were markedly lower than those of CDK4 in the parental (sensitive) models, which is also consistent with data from TCGA showing significantly higher levels of CDK4 than CDK6 transcripts in most ER^+ breast cancers but not in *FAT1* negative tumors (Figure 4E). By contrast, the expression of other components such as cyclin D1 or pRB was not consistently or significantly induced across models. Together, these data imply that CDK6 expression is frequently repressed in ER^+ breast cancers by wild-type FAT1 and that CDK4 is the dominantly expressed G_1-S kinase. In addition, we examined a pair of resistant cell lines, MR3 and MR O9, that were generated by chronically exposing MCF7 cells to abemaciclib for 6 months and collecting different clones (Yang et al., 2017). These cell lines showed marked suppression of FAT1 levels (Figure S4A). We examined CDK4 and CDK6 levels in these cells and again found the suppression of FAT1 was strongly correlated with relatively high levels of CDK6 compared to parental MCF7s (Figure 4F, Figure S4A). We and others have previously established that such elevated levels of CDK6 can promote resistance to antiestrogens (Alves et al., 2016) and CDK4/6 inhibitors (Yang et al., 2017).

To determine whether the levels of CDK6 kinase induced by *FAT1* loss might be sufficient to promote resistance to CDK4/6i, we utilized short hairpin RNAs that target the 3' UTR of the *CDK6* mRNA thereby suppressing CDK6 protein to parental levels and rescued this with overexpression of wild-type CDK6 cDNA. We observed that CDK6 knockdown restored the ability of abemaciclib (100 nM) to fully inhibit cell proliferation and Rb phosphorylation, while CDK6 overexpression reinforced drug insensitivity (Figure 4G, Figure S4B).

Finally, we sought to determine if there was evidence for CDK6 upregulation in FAT1 low tumors from patients. We utilized an ER^+ patient derived xenograft (PDX) model that displays initial sensitivity to CDK4/6i therapy with heterogeneous development of drug resistance (Figure 4H) and examined FAT1 and CDK6 levels by immunohistochemistry (IHC) (Figure 4I). We performed IHC on tumors after 9 weeks on ribociclib therapy and found that resistant tumors harbored low cytoplasmic and membranous FAT1 expression while sensitive tumors had strong FAT1 expression. Correspondingly, the FAT1-low PDXs all displayed high levels of CDK6 expression while the FAT1 high tumors did not. The protein levels of FAT1 and CDK6 in these PDXs were also detected by immunoblot (Figure S4C). Consistent with the IHC result, PDXs that developed resistance showed decreased FAT1 expression and induction of CDK6 expression compared to PDXs that remained sensitive. In keeping with these findings, matched tumor samples from *FAT1* negative tumors (Fig 2) showed low FAT1 by IHC and strong CDK6 expression (Figure 4J, Figure

S4D). For comparison, a group of wild-type *FAT1* patient tumors showed high FAT1 and relatively low CDK6 expression by IHC (Figure 4J, Figure S4D). The average quantitative IHC score showed significantly lower FAT1 and higher CDK6 in *FAT1* mutated patient tumors when compared with those with wild-type (Figure S4E). Taken together, the data demonstrate a highly consistent upregulation of CDK6 levels among *FAT1* loss or suppressed tumors.

FAT1 regulates CDK6 via the Hippo pathway

To understand the mechanisms by which FAT1 regulates CDK6 expression, we noted prior studies that had implicated the β-catenin signaling pathway (Morris et al., 2013) or the Hippo pathway (Martin et al., 2018) as potential effectors of FAT1 in head and neck cancers. In addition, studies in non-cancerous cells have implicated FAT1 as an occasional activator of Hippo signaling (Ahmed et al., 2015; Bennett and Harvey, 2006; Cho et al., 2006; Silva et al., 2006; Skouloudaki et al., 2009; Tyler and Baker, 2007; Willecke et al., 2006). To determine whether FAT1 regulates CDK6 in breast cancer cells via either of these pathways, we assessed multiple canonical transcriptional targets of these networks by qPCR in parental and *FAT1*-loss cells (Figure 5A). Whilst the expression of Wnt/β-catenin targets *AXIN2* and *MYC* were unaffected by *FAT1* loss, marked upregulation of *CTGF* and *CYR61* was detected, consistent with downregulation of Hippo signaling (Figure 5A). To ascertain whether canonical Wnt/β-catenin signaling would be necessary and sufficient for the *FAT1* loss-mediated effects, we knocked down β-catenin in the *FAT1*-loss cells and drug-resistant cells and observed no significant impact upon abemaciclib sensitivity and CDK6 protein level (Figure S5A). We next examined whether inhibition of Hippo pathway effectors YAP and/or TAZ (encoded by *WWTR1*) might impact the induction of CDK6 in *FAT1*-loss cells (Figure 5B, Figure S5B). These data reveal that knockdown of YAP1 alone or together with TAZ consistently suppressed the induction of canonical targets like *CTGF* as well as *CDK6* (Figure 5B, Figure S5B) and restored the sensitivity of *FAT1*-loss cells to CDK4/6i (Figure 5C). As the data pointed to YAP/TAZ as essential mediators of the *CDK6* induction, we sought to identify the basis for how these transcription factors might impact CDK6 in breast cancer cells. Based on previous studies, two canonical TEAD binding sites were identified in the *CDK6* promoter (Xie et al., 2013) (Figure 5D). We assessed YAP/TAZ binding at these sites using a ChIP-qPCR assay and found marked enrichment of both YAP and TAZ in *FAT1* loss cells compared to parental (Figure 5D). Moreover, introduction of a dominant-negative (DN) TEAD construct abrogated the induction of CDK6 (Figure S5C). In addition, to ascertain whether FAT1 is sufficient to suppress the transcription of *CDK6* and other Hippo pathway targets in breast cancer cells, we expressed the intracellular domain of FAT1 (CD4-FAT1-ICD)(Martin et al., 2018) in *FAT1* knockout cells. As expected, we found expression of just a portion of FAT1 partially suppresses *CDK6* transcription along with multiple Hippo targets, including *AREG, CYR61*, and *BIRC5*, further supporting the role of FAT1 in regulation of *CDK6* through the Hippo pathway (Figure S5D). To further confirm the association of FAT1 with activation of YAP, we examined YAP localization utilizing immunofluorescence and found that FAT1 knockdown cells demonstrated strong nuclear localization of YAP compared to parental cells (Figure 5E). We similarly found increased YAP nuclear localization in FAT1-low PDX models and FAT1-low human breast tumors (Figure S5E, F). Finally, we examined components of the Hippo signaling pathway upstream

of YAP and found suppression of Hippo signaling (loss of MST1 and LATS1 phosphorylation) in *FAT1* knockout cells and FAT1-low PDXs (Figure 5F, Figure S4C), consistent with *FAT1* loss causing Hippo pathway suppression and YAP/TAZ activation.

To examine this in the whole transcriptome scale, we performed RNA-seq on *FAT1* knockout cell lines compared to wild-type. We indeed identify upregulation of *CDK6* and *CTGF* mRNA as a result of *FAT1* knockout (Figure 5G, Table S5). Moreover, in performing gene set enrichment analysis using GSEA, we indeed find a statistically significant enrichment of Hippo pathway regulated genes (Figure 5G) in FAT1 negative models.

Hippo pathway alterations and drug resistance

We hypothesized that other oncologic mechanisms involving constitutive suppression of Hippo signaling might also lead to CDK4/6i resistance in breast cancer cells in a manner akin to *FAT1* loss. Like FAT1, Merlin (encoded by *NF2*) (Cooper and Giancotti, 2014), is a known tumor suppressor that regulates Hippo signaling and is localized to the membrane. Indeed, subcellular localization of NF2 and FAT1 by immunofluorescence demonstrated the proteins to be colocalized at the plasma membrane (Figure 6A). To determine if *NF2* loss might recapitulate the effects of *FAT1* loss, we generated two models of *NF2* knockout by CRISPR in MCF7 cells. In this case, pools of cells with knockout were generated and suppression of NF2 levels (85%) was confirmed by immunoblotting (Figure 6B). As with FAT1, the CDK6 levels were significantly higher in the *NF2* knockout cells than in parental cells (Figure 6B, C). Once again, NF2 loss and high CDK6 were associated with lack of growth inhibition by CDK4/6i (abemaciclib) (Figure 6D). Based on these findings, we posited that other oncogenic alterations in Hippo signaling might also be associated with drug resistance in the clinic. Consistent with our hypothesis, genomic alterations in the Hippo pathway, albeit individually rare (Figure 6E), were collectively associated with reduced response to CDK4/6i in ER^+ metastatic breast cancer patients (hazard ratio: 3.6; 95% CI: 1.7, 7.8, p value = $4.4x10^{-4}$, Figure 6F, Table S6). These data thus suggest that intact signaling of the Hippo pathway and low CDK6 levels may be an additional basis for why CDK4/6i are so broadly effective in many patients with ER^+ breast cancers.

DISCUSSION

CDK4/6 inhibitors have demonstrated remarkable clinical activity in ER^+ breast cancer and have transformed the treatment paradigm for this highly prevalent disease. Despite this impact, intrinsic and acquired resistance to these drugs is widespread and poorly understood. Through a biology-driven genomic survey of patients treated with these drugs, we have identified loss of the *RB1* and *FAT1* tumor suppressors as recurrent mechanisms of resistance to CDK4/6i. Whilst the finding of *RB1* loss was anticipated based on Rb's canonical role as a CDK4/6 substrate, the link between FAT1 and CDK4/6 activity was not previously appreciated. In this report, we establish that FAT1 can regulate cancer cell proliferation through activation of the Hippo signaling pathway and the CDK6 kinase. Together, the data point to suppression of the Hippo signaling pathway as a potentially common mechanism of cancer cell proliferation and resistance to CDK4/6 inhibitors, nominate *RB1* and Hippo pathway components as potential biomarkers for cancer therapy

selection, and imply more potent inhibitors of CDK6 may be valuable as strategies for overcoming drug resistance.

One of the challenges in sorting through very large gene sets to identify important associations of genetic alterations with clinical outcomes is the difficulty of annotating large tumor suppressors whose functions and domains have not been fully mapped. To identify mutations associated with resistance to CDK4/6 inhibitors, we specifically sought to establish whether loss of any tumor suppressors might be relevant. At variance with oncogenes, tumor suppressors often lack hotspot mutations, and have a spectrum of single nucleotide variants and small insertions and deletions distributed across the entire coding region of the gene. These characteristics render the discovery of potential roles for these genes as drivers of specific biologic phenomena challenging. This is particularly the case in the context of resistance to therapy, which is often a convergent phenotype (i.e. caused by a repertoire of somatic genetic alterations) where the contribution of each individual gene may be small. In this setting, algorithms to define significantly mutated genes based on the frequency of recurrence of alterations affecting a given gene do not perform well. To avoid variants of uncertain significance obscuring our findings, particularly for large genes including *FAT1*, we chose to establish stringent criteria in which only likely pathogenic mutations (nonsense, frameshift and splice site somatic mutations or homozygous deletions) for known tumor suppressors were included in our screen. This approach is undoubtedly conservative, and we accept that some missense variants excluded from the analyses may have a biological impact. Based on previous observations related to tumor suppressor genes where the effect of individual mutations can be quantified genomically, however, the number of biologically-relevant missense mutations in classical tumor suppressor genes is likely small (Riaz et al., 2017). It should be noted that the two independent approaches employed in this study for the classification of mutations as pathogenic resulted in the identification of both an expected (*RB1*) and a previously unidentified (*FAT1*) gene associated with lack of response to CDK4/6i. With the increasing utilization of large gene panels for studying various disease associations, these complementary analytical approaches may prove valuable to many investigators, particular as it relates to poorly studied genes.

The specific finding of *FAT1* and *RB1* associated with short PFS was quite robust in our large cohort. Patients with deleterious mutations in these genes derived virtually no benefit from CDK4/6i, nearly always progressing on therapy at the time of their first radiologic assessment. The fact that these mutations were not highly prevalent in our cohort or TCGA broadly is entirely consistent with the wide activity of CDK4/6 inhibitors in the clinic (Dickler et al., 2017; Finn et al., 2016; Hortobagyi et al., 2016; Sledge et al., 2017; Turner et al., 2015). However, the patients who receive these drugs do very commonly experience disease recurrence after 1–3 years on therapy and, based upon our findings, are also likely to have alterations in these genes. Indeed, two recent reports (Condorelli et al., 2018; O'Leary et al., 2018) identified a few cases of acquired alterations in *RB1*. Moreover, there does exist a group of patients previously untreated with CDK4/6 inhibitors who harbor readily detectable alterations in either *FAT1* or *RB1* and who might be candidates for other currently available and approved forms of therapy than CDK4/6 inhibitors.

The clinical finding of *RB1* loss associated with resistance to CDK4/6 inhibitors is of course anticipated based on Rb being the major target of CDK4/6 kinase and the role of unphosphorylated Rb in suppressing E2F and transcription. However, the link between *FAT1* and CDK4/6 was completely unknown and led us to investigate its basis. We were quite surprised to find that, similar to our previous study in which *CDK6* amplification caused CDK4/6i resistance cell line models, we found that FAT1 also directly regulated transcription of *CDK6*. In fact, one of the cell line models we originally identified (MR) to have high levels of CDK6 protein but no *CDK6* amplification was subsequently shown to have downregulation of FAT1 expression. The essential role of CDK6 in this scenario was proven through a number of studies including knockdown of CDK6 restoring drug sensitivity, overexpression of CDK6 causing resistance, and more potent drug inhibition of CDK6 kinase achieving inhibition of cell growth. The pharmacologic implication of these results is intriguing– bacterial-derived CDK6 kinase is a highly sensitive target of all three FDA-approved CDK4/6 inhibitors, and recent data has shown that certain rare tumor types with high level CDK6-cyclinD3 can be highly sensitive to CDK4/6 inhibition. These data raise the question as to whether CDK4 and CDK6 in cells might be found in different complexes and thereby harbor different sensitivities. We have preliminary evidence for this in identifying a markedly different partition of proteins associated with CDK4 versus CDK6 from ER^+ breast cancer cells (data not shown). We speculate that distinct CDK4 and CDK6 complexes will represent an additional and important parameter in understanding the underlying sensitivity of most ER^+ breast cancers to CDK4/6i.

The finding that CDK6 kinase was responsible for drug resistance in the *FAT1*-loss cells helped to explain one fundamental aspect of drug resistance but did not explain how the membrane-localized FAT1 was linked to *CDK6* transcription. To understand this, we interrogated the pathways that the FAT1 ortholog is linked to in Drosophila, β-catenin and Hippo signaling. Whilst β-catenin signaling has been previously linked to cell cycle progression and breast cancer tumor growth, little is known about Hippo signaling in ER^+ breast cancers. Nevertheless, our data from multiple cell line models revealed that it is in fact the Hippo pathway that is suppressed as a consequence of *FAT1* loss and this directly leads to CDK6 upregulation. The link between Hippo and CDK6 is directly mediated by the YAP and TAZ transcription factors that bind the CDK6 promoter upon activation and cause its upregulation. Naturally, other effects of YAP and TAZ activation are likely to be of some importance in these cells (Chan et al., 2008), but we find the upregulation of CDK6 to be both necessary and sufficient for the effects on drug sensitivity. It remains to be understood how FAT1 specifically connects to the Hippo pathway in breast cancer cells, and this may yield additional therapeutic considerations for ultimately drugging this pathway in patients.

Altogether, our data point to a number of potential genetic mechanisms that could dysregulate Hippo signaling and lead ultimately to CDK6 overexpression and resistance to CDK4/6 inhibitors in patients. Beyond *FAT1* loss, alterations in *YAP*, *MST1*, *LATS1*, and *NF2* might have this potential effect and will need to be examined in greater detail going forward. The potential importance of this pathway is likely to extend beyond CDK4/6 inhibitor resistance as these lesions were observed in cases unexposed to CDK4/6 inhibitors as well as many other cancers, implying additional oncogenic functions. However, the role

of CDK6 itself appears central to this tumor suppressor network and suggest that targeting CDK6 is likely be more broadly relevant in cancer than previously appreciated.

STAR METHODS

CONTACT FOR REAGENT AND RESOURCE SHARING

Further information and requests for resources and reagents should be directed to and will be fulfilled by the Lead Contact, Sarat Chandarlapaty (chandars@mskcc.org).

EXPERIMENTAL MODEL AND SUBJECT DETAILS

Human subjects—A total of 431 breast tumor specimens from 378 patients with HR^+/$HER2^-$ metastatic breast cancer who received CDK4/6 inhibitors in combination with hormonal therapy in metastatic setting underwent prospective clinical genomic profiling between April 2014 and March 2017. This study was approved by the Memorial Sloan Kettering Cancer Center Institutional Review Board (IRB) and all patients provided written informed consent for tumor sequencing and review of patient medical records for detailed demographic, pathologic, and treatment information (NCT01775072). Detailed treatment history data were obtained for each patient and included all lines of systemic therapy from time of diagnosis of invasive carcinoma to the study data lock in September 2017. The exact regimen as well as the dates of start and stop of therapy were recorded for each treatment line. For each treatment line, the time of biopsy collection for MSK-IMPACT testing was compared with the treatment start and stop dates. We excluded samples that were collected after the start of CDK4/6 inhibitor therapy (n = 52 samples) and only included samples that were collected prior or within the first 60 days of therapy initiation. We also excluded samples that were collected prior to CDK4/6 inhibitors as part of an unpublished clinical trial (n= 1). The final cohort included 348 patients. The demographic and clinical characteristics of the cohort is presented in Table S1.

Cell lines—MCF7 (RRID:CVCL_0031; female), CAMA-1 (RRID:CVCL_1115; female), HEK 293T (RRID:CVCL_0063; female) and MCF7 derived cells (MCF7 FAT1-CR-1/2/3, MCF7 FAT1-sh-A/B, MCF7 FAT1-CR-1 shCDK6, MCF7 FAT1-CR-1 shCDK6+CDK6 rescue, MCF7 FAT1-CR-1 shYAP1, MCF7 FAT1-CR-1 shTAZ, MCF7 FAT1-CR-1 shYAP1+shTAZ, MCF7 FAT1-CR-1 CD4-FAT1-ICD rescue, MCF7 RB1-sh, MCF7 CDK6-N1, MCF7 NF2-CR-A/B, MR3 and MR O9) were maintained in DMEM/F12. T47D (RRID:CVCL_0553; female) and ZR-75–1 (RRID:CVCL_0588; female) cells were maintained in RPMI. All cell lines were maintained in a humidified atmosphere with 5% CO2 at 37 °C. All media were supplemented with 10% FBS, 2 mM L-glutamine, 20 units/ml penicillin and 20 μg/ml streptomycin. STR genotyping of all cell lines used in this study was previously performed to validate cell line identity.

In Vivo Tumor Models—All mouse studies were conducted through Memorial Sloan Kettering Cancer Center and performed in compliance with institutional guidelines under an institutional animal care and use committee (IACUC)-approved protocol (MSKCC 12–10-016). Patient consent for tumor use in animals was obtained under a protocol approved by the Memorial Sloan Kettering Cancer Center IRB (IRB#13–040). PDXs were derived

from an $ER^+/HER2^-$ breast cancer patient. Tumors were subcutaneously implanted in 6-week old NSG female mice (RRID:IMSR_JAX:005557) and treated with vehicle or ribociclib (200 mg/kg) via oral gavage daily. Tumor volumes and weights were measured twice a week. All tumors would be collected to detect mRNAs and proteins levels at the end of treatment.

METHOD DETAILS

Prospective sequencing and analysis—For all 348 patients, tumor and patient-matched normal DNA samples were extracted from either representative formalin-fixed paraffin embedded (FFPE) tumor biopsy samples or mononuclear cells from peripheral blood. All specimens underwent massively parallel next-generation sequencing in a CLIA-certified laboratory using MSK-IMPACT, a hybridization capture-based next-generation sequencing assay, which analyzes all protein-coding exons and selected intronic and regulatory regions of 341 to 468 cancer-associated genes (Table S2), all as previously described (Cheng et al., 2015; Razavi et al., 2018; Zehir et al., 2017). Samples were sequenced using either the 341-gene version 1 panel (n=49); the 410-gene version 2 panel (n=247); or the 468-gene version 3 panel (n=52). Average sequencing coverage across all tumors was 743-fold. Somatic mutations, DNA copy number alterations, and structural rearrangements were identified as previously described (Cheng et al., 2015) and all mutations were manually reviewed (Table S2). In addition to the gene-level amplification and deletion calls generated by the clinical laboratory pipeline, genome-wide total and allele-specific DNA copy number was determined using the FACETS (Shen and Seshan, 2016). Purity, average ploidy, and allele-specific integer-copy number for each segment were then determined by maximum likelihood. Loss of heterozygosity (LOH) was determined based on allele-specific integer-copy number for tumor suppressors.

Quantitative RT-PCR and chromatin immunoprecipitation (ChIP)—Quantitative RT-PCR was performed as described previously (Yang et al., 2017). Briefly, total RNA was extracted using QIAGEN RNeasy kit (Qiagen, Venlo, Netherlands). RNA (1 μg) was reverse-transcribed into cDNA using qScript cDNA SuperMix (Quanta Biosciences, Beverly, MA, USA). qPCR reactions were performed with TaqMan PCR Master Mix (Applied Biosystems, Foster City, CA, USA) using a ViiA 7 Real-Time PCR system (Applied Biosystems) along with primers. Samples were run in triplicate, and mRNA levels were normalized to those of *RPLP0* for each reaction. Taqman primers were purchased from Applied Biosystems and included: FAT1 (Hs00170627_m1), CDK4 (Hs01565683_g1), CDK6 (Hs01026371_m1), CCND1 (Hs00765553_m1), CCNE2 (Hs00180319_m1), E2F1 (Hs00153451_m1), RB1 (Hs01078066_m1), YAP1 (Hs00902712_g1), TAZ (Hs00210007_m1), CTGF (Hs01026927_g1), CYR61 (Hs00155479_m1), AXIN2 (Hs00610344_m1) and RPLP0 (Hs99999902_m1), NF2 (Hs00966302_m1).

ChIP assay was performed as described previously (Bosch et al., 2015). Briefly, cells were crosslinked and collected. Chromatin was broken down into 200–1000 bp fragments through 30 minutes sonication. 1% of total chromatin was used as input. Chromatin was incubated overnight at 4°C with 1 μg of antibody. 20 μl ChIP grade magnetic beads (Thermo Fisher Scientific, Waltham, MA, USA) were added into each IP tube and incubated for 2 hours. IP

samples were washed and crosslinks were reversed by heating at 65°C overnight with Proteinase K. Chromatin was purified using Qiagen PCR purification kit (Qiagen). Primers sequences used for ChIP were: CDK6 ChIP, forward: 5'- ACTGGACCGGGCCTTTAG -3', reverse: 5'- GAGAAGGTCTCTGTCCTC -3' (Xie et al., 2013). Signals of ChIP samples were normalized to their respective input signals.

Lentiviral infection and generation of stable cell lines—HEK293T cells were used to package virus. 2×10^7 cells were plated in 10 cm tissue culture dish and transfected with 4.5 μg of the SGEP or SGEN lentiviral vector (encoding shRenilla, or target shRNAs), 4.5 μg of psPAX2 and 1 μg of pVSVG with X-tremeGENE HP (Roche) according to the manufacturer's protocol. Conditioned medium containing recombinant lentiviruses was collected 48 hours after transfection and filtered through non-pyrogenic filters with a pore size of 0.45 μm (Merck Millipore, Billerica, MA, USA). Samples of these supernatants were applied immediately to target cells together with Polybrene (Sigma-Aldrich, St. Louis, MO, USA) at a final concentration of 8 μg/ml, and supernatants were incubated with cells for 12 hr. After infection, cells were placed in fresh growth medium and cultured as usual. Selection with 2 μg/ml puromycin (Thermo Fisher Scientific) or 1 mg/ml G418 (InvivoGen, San Diego, CA, USA) was initiated 48 h after infection.

Cloning and plasmids—lentiCRISPRv2 one vector system was used to establish all knockout cells. lentiCRISPR v2 was a gift from Feng Zhang (Addgene plasmid # 52961) (Sanjana et al., 2014). FAT1-CRISPR plasmid was a gift from the Timothy A. Chan lab. Single guide RNAs were designed through MIT CRISPR Designer (crispr.mit.edu) and the sequences are: FAT1-CRISPR: CACGGTGACGTTGTACTCGG; NF2-CRISPR: GAACTCCATCTCGGCGTCCA. Cloning strategy was described previously (Shalem et al., 2014). Oligos were annealed and ligated with BsmBI digested lentiviral vector. Then the ligation system was transformed into Stbl3 bacteria and plasmids were extracted for sequencing.

FAT1-shRNA plasmids, FAT1-sh-A (TRCN0000038024) and FAT1-sh-B (TRCN0000245156), were obtained from Sigma-Aldrich. *Renilla*, CDK6, YAP1 and TAZ shRNAs were put into mir-E, an optimized microRNA backbone, as previously described (Fellmann et al., 2013). Hairpin ultramers were amplified and put into lentiviral SGEP or SGEN vector, which are gifts from the Charles Sawyers lab. Proper insertions were verified by Sanger sequencing. shRNA sequences are: Renilla-sh:

TGCTGTTGACAGTGAGCGCAGGAATTATAATGCTTATCTATAGTGAAGCCACAGAT GTATA GATAAGCATTATAATTCCTATGCCTACTGCCTCGGA; CDK6-sh:

TGCTGTTGACAGTGAGCGCTAGGTGTTGTCAGTACTATAATAGTGAAGCCACAGAT GTATT ATAGTACTGACAACACCTAATGCCTACTGCCTCGGA; YAP1-sh:

TGCTGTTGACAGTGAGCGCTAGAGTAGTAATGAAATTCTATAGTGAAGCCACAGAT GTATA GAATTTCATTACTACTCTAATGCCTACTGCCTCGGA; TAZ-sh:

TGCTGTTGACAGTGAGCGCCCGGAAGACTCTGTTGTAGAATAGTGAAGCCACAGA TGTATT CTACAACAGAGTCTTCCGGTTGCCTACTGCCTCGGA

CDK6 sequence from pDONR223-CDK6 (a gift from William Hahn & David Root; Addgene plasmid # 23688) was delivered into pLenti PGK Neo DEST (w531–1) (a gift from Eric Campeau & Paul Kaufman; Addgene plasmid # 19067) by using the Gateway LR Clonase II Enzyme Mix (Invitrogen, Waltham, MA, USA) and used for CDK6 overexpression in FAT1-CR-1/shCDK6 cells. Chimeric CD4-FAT1 sequence was generated by Genewiz and cloned into pLX302, a gift from David Root (Addgene plasmid # 25896).

Immunohistochemistry (IHC)—Immunohistochemistry was performed by Ventana BenchMark ULTRA Automated Stainer. The primary antibodies were hand-applied to the slides (FAT1 2ug/ml, CDK6 1ug/ml) followed by a OmniMap HRP multimer detection system (DISCOVERY, Basel, Switzerland). Evaluation of FAT1 and CDK6 staining was recorded as positive staining according to the status of the cell membrane and cytoplasmic signals. Staining intensity (0, 1, 2, 3) and percentage of positive cells among cancer duct (0–25% recorded as 1, 25–50% as 2, 50–75% as 3 and >75% as 4) were evaluated by a pathologist in MSKCC. The final immunoreactive scores were calculated by multiplying the two numbers as described before (Li et al., 2016).

Immunofluorescent and confocal microscopy—MCF-7 parental and Fat1 crispr cells were cultured and fixed on the 8-chamber slide. Cells were permeablized by 0.1% Triton X-100 and blocked by 10% goat serum before incubation with primary antibodies. Fat1 (HPA001869; Sigma-Aldrich) and NF2 (Merlin, ab88957; Abcam) were used. Secondary antibodies (goat anti-mouse Alexa 488 and goat anti-rabbit Alexa 594) were from Invitrogen. Cell nucleus were counterstained with DAPI. Images were acquired under a point-scanning confocal microscope on an upright stand (Zeiss).

Cell proliferation—Cell proliferation was measured as described previously (Yang et al., 2017). Briefly, for long term culture (35 days), cells (300/well) were seeded into 96-well plates and treated with different concentrations of indicated drugs. Media and drug were changed every week. On Day 0, 7, 14, 21, 28 and 35, 25 μl of Resazurin (R&D Systems, Minneapolis, MN, USA) was added to each well and incubated for 4 hours. Fluorescence in the plate was measured using a microplate reader (SpectraMax M5, Molecular Devices, Sunnyvale, CA, USA). For short term culture, cells (1×10^3/well) were seeded into 96-well plates and treated with different concentrations of indicated drugs. On Day 0, 3, 5 and 7, 25 μl of Resazurin (R&D Systems, Minneapolis, MN, USA) was added to each well and incubated for 4 hours. Fluorescence in the plate was measured using a microplate reader (SpectraMax M5, Molecular Devices, Sunnyvale, CA, USA). Cell growth data from Day 5 was then plotted as percentage inhibition against the log concentration of indicated drug. IC_{50} was determined using a sigmoidal regression model using GraphPad Prism 7.0.

Immunoblotting—Cells were lysed in RIPA buffer (Thermo Fisher Scientific) supplemented with protease and phosphatase inhibitors (Pierce) and were sonicated briefly for 30 s. Lysates were centrifuged at maximum speed for 10 min, and protein concentration was determined using the BCA kit (Fisher Scientific). For each sample, 60 μg of protein lysate was loaded onto 4–12% SDS-PAGE minigels (Invitrogen) for electrophoresis and immunoblotting.

RNA sequencing—RNA was extracted from MCF7 cells or FAT1-CR-1 cells using the RNeasy Mini kit (Qiagen) according to the manufacturer's protocol. RNA samples were quantified using Qubit 2.0 Fluorometer (Life Technologies, Carlsbad, CA, USA) and RNA integrity was checked with 4200 TapeStation (Agilent Technologies, Palo Alto, CA, USA). RNA sequencing library preparation used the NEBNext Ultra RNA Library Prep Kit for Illumina followed by manufacturer's instructions (NEB, Ipswich, MA, USA). Sequencing was done on the Illumina HiSeq instrument using a 2x150 Paired End (PE) configuration with 30–40 million reads per sample by GENEWIZ, LLC. (South Plainfield, NJ, USA).

QUANTIFICATION AND STATISTICAL ANALYSIS

Functional evaluation of alterations

Integrative pathway analysis: For each gene, oncogenic relevance of specific variants and copy number changes was assessed using the latest versions of the OncoKB (Chakravarty et al., 2017) [www.oncokb.org] and cancer hotspots (Chang et al., 2016) [www.cancerhotspots.org] knowledge bases (Tables S2, S3). For known oncogenes, only somatic genetic alterations inferred to be activating were considered; for genes with tumor suppressive roles alterations inferred to be inactivating were considered only if allele-specific copy number analysis showed evidence of LOH of the wild-type allele (Shen and Seshan, 2016).

As a second and orthogonal approach to differentiate between likely passenger and likely driver genetic alterations, we employed a combination of mutation function predictors as previously described (Martelotto et al., 2014) (Table S2, S3). Missense SNVs defined as non-deleterious/ passenger by both MutationTaster (Schwarz et al., 2010) and CHASM (breast) (Carter et al., 2009), a combination of mutation function predictors shown to have a high negative predictive value (Martelotto et al., 2014), were considered likely passenger alterations. The remaining missense SNVs were defined as likely pathogenic if they affected hotspot residues (Chang et al., 2016), or were predicted to be "driver" and/or "cancer" by CHASM (breast classifier) and/or FATHMM (Shihab et al., 2013), respectively, or affected cancer genes included in the cancer gene lists described by Kandoth et al. (127 significantly mutated genes) (Kandoth et al., 2013) the Cancer Gene Census (Futreal et al., 2004) or Lawrence et al. (Cancer5000-S gene set) (Lawrence et al., 2014). In-frame indels defined as "neutral" by MutationTaster (Schwarz et al., 2010) and PROVEAN (Choi et al., 2012) were defined as likely passengers as previously described (Zehir et al., 2017). The remaining in-frame indels, as well as frameshift, splice-site and truncating mutations were considered likely pathogenic if they affected hotspot codons (Chang et al., 2016), or were targeted by loss of the wild-type allele or affected haploinsufficient genes or affected cancer genes (Futreal et al., 2004; Kandoth et al., 2013; Lawrence et al., 2014). Mutations that were neither likely pathogenic nor likely passenger were considered of indeterminate pathogenicity.

We investigated somatic alterations - including mutations, copy number changes and gene fusions - within the context of 7 canonical mitogenic signaling pathways as described before (Table S6) (Sanchez-Vega et al., 2018). These included cell cycle/P53, Hippo, Notch, Wnt, PI3K, RTK/RAS, TGF-Beta and oxidative stress response. The set of genes included in each

pathway was chosen based on exhaustive review of the signaling pathway literature, including a curated analysis of the compendium of pathway diagrams published in TCGA marker papers throughout the past decade. The following table summarizes the sets of genes from the MSK-IMPACT assay that were altered in at least one of our samples and that we associated to each of the ten pathways:

Pathway	Genes
Cell Cycle/P53	*CCND1, CCND2, CCND3, CCNE1, CDK4, CDK6, CDKN1A, CDKN1B, CDKN2A, CDKN2B, CDKN2C, RB1, MAX, MGA, MYC, MYCN, ATM, MDM2, MDM4, TP53*
Hippo	*FAT1, LATS1, LATS2, NF2, YAP1*
Notch	*CREBBP, EP300, FBXW7, KDM5A, NCOR1, NOTCH1, NOTCH3, SPEN*
PI3K	*AKT1, AKT2, AKT3, INPP4B, MTOR, PIK3CA, PIK3CB, PIK3R1, PIK3R2, PIK3R3, PPP2R1A, PTEN, RICTOR, STK11, TSC1, TSC2*
RTK/RAS	*ALK, ARAF, BRAF, CBL, EGFR, ERBB2, ERBB3, ERBB4, ERF, ERRFI1, FGFR1, FGFR2, FGFR3, FGFR4, FLT3, HRAS, IGF1R, INSR, JAK2, KIT, KRAS, MAP2K1, MAPK1, MET, NF1, NRAS, NTRK1, NTRK2, NTRK3, PDGFRA, PDGFRB, PTPN11, RAC1, RAF1, RASA1, RET, ROS1, SOS1*
TGF-Beta	*SMAD2, SMAD3, SMAD4, TGFBR1, TGFBR2*
Wnt	*APC, AXIN1, AXIN2, CTNNB1, RNF43, TCF7L2*
NRF2	*KEAP1, NFE2L2*

Statistical analysis: We determined the association between genomic alterations and PFS with disease progression on therapy with CDK4/6 inhibitors or patient death. We categorized CDK4/6 inhibitor regimens based on their endocrine therapy backbone to two major categories: 1) CDK4/6 inhibitors plus aromatase inhibitors (AI) including letrozole, exemestane, or anastrozole); 2) CDK4/6 inhibitors plus selective estrogen receptor degraders (SERD) including fulvestrant. We used univariate Cox proportional hazard models stratified by the treatment class (CDK4/6i+AI or CDK4/6i+SERD) to determine the association between genomic alterations in each gene or set of genes and PFS. A given gene was only included if mutations were present in at least 5 patients. For patients with multiple lines of therapy from the same class of treatment, only the first treatment line from that class that was started after the MSK-IMPACT biopsy was included in the analysis. We tested the proportionality assumption of the Cox regression model through time-dependency analysis of selected genetic alterations (cox.zph function of the R package survival). We rejected the null hypotheses with a two-sided $\alpha = 0.05$. Statistical significance was determined by log-rank test stratified by the treatment. Resulting p values were corrected for multiple hypothesis testing with Benjamini and Hochberg method.

Analysis of RNA sequencing data—The raw data were trimmed to remove possible adapter sequences and nucleotides with poor quality using Trimmomatic v.0.36 (Bolger et al., 2014). The trimmed reads were mapped to the *Homo sapiens reference* genome available on ENSEMBL using the STAR aligner v.2.5.2b (Dobin et al., 2013). Unique gene hit counts were calculated by using feature Counts from the Subread package v.1.5.2 (Liao et al., 2013; Liao et al., 2014). Only unique reads that fell within exon regions were counted. Differentially expressed genes were determined using DESeq2 (Love et al., 2014) and a cut-off of adjusted p values < 0.05 and absolute log2 fold changes > 1 was used for creating lists

unless otherwise stated. GSEA (Subramanian et al., 2005) was used to perform gene set enrichment analysis.

Statistical analysis for experimental data: The details of statistical analysis of experiments can be found in the figure legends. Statistical analysis of differences between samples was performed using two-tailed Student's t-tests, and $p < 0.05$ was defined as significant. When comparing various groups one-way ANOVA statistical test was used applying the Dunnett's method or Tukey's method to correct for multiple comparisons. The analysis was conducted using GraphPad Prism 7.0. Independent experiments were conducted with a minimum of two biological replicates per condition to allow for statistical comparison. Data is shown as mean ± SD.

DATA AND SOFTWARE AVAILABILITY

The mutational data is publicly available through the cBioPortal for Cancer Genomics (http://www.cbioportal.org/study?id=breast_msk_2018) and is also deposited in the European Variation Archive (EVA). The accession number for the sequencing data is PRJEB29597, https://www.ebi.ac.uk/eva/?eva-study=PRJEB29597. The accession number for the deposited RNA sequencing data reported in this paper is GEO: GSE122088.

Supplementary Material

Refer to Web version on PubMed Central for supplementary material.

Acknowledgments

We would like to thank T. Chan for plasmids and oligonucleotides. We would also like to thank Andy Koff for his helpful discussions. This work was funded by the generous support of the Cancer Couch Foundation, the Shen Family Fund, the Weinberg Family Fund, the Breast Cancer Research Foundation, the Breast Cancer Alliance Young Investigator Award, and the NCI Cancer Center Support Grant (CCSG, P30 CA08748).

REFERENCES

Ahmed AF, de Bock CE, Lincz LF, Pundavela J, Zouikr I, Sontag E, Hondermarck H, and Thorne RF (2015). FAT1 cadherin acts upstream of Hippo signalling through TAZ to regulate neuronal differentiation. Cell Mol Life Sci 72, 4653–4669. [PubMed: 26104008]

Alves CL, Elias D, Lyng M, Bak M, Kirkegaard T, Lykkesfeldt AE, and Ditzel HJ (2016). High CDK6 Protects Cells from Fulvestrant-Mediated Apoptosis and is a Predictor of Resistance to Fulvestrant in Estrogen Receptor-Positive Metastatic Breast Cancer. Clin Cancer Res 22, 5514–5526. [PubMed: 27252418]

Bennett FC, and Harvey KF (2006). Fat cadherin modulates organ size in Drosophila via the Salvador/Warts/Hippo signaling pathway. Curr Biol 16, 2101–2110. [PubMed: 17045801]

Bolger AM, Lohse M, and Usadel B (2014). Trimmomatic: a flexible trimmer for Illumina sequence data. Bioinformatics 30, 2114–2120. [PubMed: 24695404]

Bosch A, Li Z, Bergamaschi A, Ellis H, Toska E, Prat A, Tao JJ, Spratt DE, Viola-Villegas NT, Castel P, et al. (2015). PI3K inhibition results in enhanced estrogen receptor function and dependence in hormone receptor-positive breast cancer. Sci Transl Med 7, 283ra251.

Carter H, Chen S, Isik L, Tyekucheva S, Velculescu VE, Kinzler KW, Vogelstein B, and Karchin R (2009). Cancer-specific high-throughput annotation of somatic mutations: computational prediction of driver missense mutations. Cancer Res 69, 6660–6667. [PubMed: 19654296]

Chakravarty D, Gao J, Phillips SM, Kundra R, Zhang H, Wang J, Rudolph JE, Yaeger R, Soumerai T, Nissan MH, et al. (2017). OncoKB: A Precision Oncology Knowledge Base. JCO Precis Oncol 2017.

Chan SW, Lim CJ, Guo K, Ng CP, Lee I, Hunziker W, Zeng Q, and Hong W (2008). A role for TAZ in migration, invasion, and tumorigenesis of breast cancer cells. Cancer Res 68, 2592–2598. [PubMed: 18413727]

Chang MT, Asthana S, Gao SP, Lee BH, Chapman JS, Kandoth C, Gao J, Socci ND, Solit DB, Olshen AB, et al. (2016). Identifying recurrent mutations in cancer reveals widespread lineage diversity and mutational specificity. Nat Biotechnol 34, 155–163. [PubMed: 26619011]

Cheng DT, Mitchell TN, Zehir A, Shah RH, Benayed R, Syed A, Chandramohan R, Liu ZY, Won HH, Scott SN, et al. (2015). Memorial Sloan Kettering-Integrated Mutation Profiling of Actionable Cancer Targets (MSK-IMPACT): A Hybridization Capture-Based Next-Generation Sequencing Clinical Assay for Solid Tumor Molecular Oncology. J Mol Diagn 17, 251–264. [PubMed: 25801821]

Cho E, Feng Y, Rauskolb C, Maitra S, Fehon R, and Irvine KD (2006). Delineation of a Fat tumor suppressor pathway. Nat Genet 38, 1142–1150. [PubMed: 16980976]

Choi Y, Sims GE, Murphy S, Miller JR, and Chan AP (2012). Predicting the functional effect of amino acid substitutions and indels. PLoS One 7, e46688. [PubMed: 23056405]

Condorelli R, Spring L, O'Shaughnessy J, Lacroix L, Bailleux C, Scott V, Dubois J, Nagy RJ, Lanman RB, Iafrate AJ, et al. (2018). Polyclonal RB1 mutations and acquired resistance to CDK 4/6 inhibitors in patients with metastatic breast cancer. Ann Oncol 29, 640–645. [PubMed: 29236940]

Cooper J, and Giancotti FG (2014). Molecular insights into NF2/Merlin tumor suppressor function. FEBS Lett 588, 2743–2752. [PubMed: 24726726]

DeCaprio JA, Ludlow JW, Lynch D, Furukawa Y, Griffin J, Piwnica-Worms H, Huang CM, and Livingston DM (1989). The product of the retinoblastoma susceptibility gene has properties of a cell cycle regulatory element. Cell 58, 1085–1095. [PubMed: 2673542]

Dickler MN, Tolaney SM, Rugo HS, Cortes J, Dieras V, Patt D, Wildiers H, Hudis CA, O'Shaughnessy J, Zamora E, et al. (2017). MONARCH 1, A Phase II Study of Abemaciclib, a CDK4 and CDK6 Inhibitor, as a Single Agent, in Patients with Refractory HR(+)/HER2(-) Metastatic Breast Cancer. Clin Cancer Res 23, 5218–5224. [PubMed: 28533223]

Dobin A, Davis CA, Schlesinger F, Drenkow J, Zaleski C, Jha S, Batut P, Chaisson M, and Gingeras TR (2013). STAR: ultrafast universal RNA-seq aligner. Bioinformatics 29, 15–21. [PubMed: 23104886]

Fellmann C, Hoffmann T, Sridhar V, Hopfgartner B, Muhar M, Roth M, Lai DY, Barbosa IA, Kwon JS, Guan Y, et al. (2013). An optimized microRNA backbone for effective single-copy RNAi. Cell Rep 5, 1704–1713. [PubMed: 24332856]

Finn RS, Crown JP, Lang I, Boer K, Bondarenko IM, Kulyk SO, Ettl J, Patel R, Pinter T, Schmidt M, et al. (2015). The cyclin-dependent kinase 4/6 inhibitor palbociclib in combination with letrozole versus letrozole alone as first-line treatment of oestrogen receptor-positive, HER2-negative, advanced breast cancer (PALOMA-1/TRIO-18): a randomised phase 2 study. Lancet Oncol 16, 25–35. [PubMed: 25524798]

Finn RS, Martin M, Rugo HS, Jones S, Im SA, Gelmon K, Harbeck N, Lipatov ON, Walshe JM, Moulder S, et al. (2016). Palbociclib and Letrozole in Advanced Breast Cancer. N Engl J Med 375, 1925–1936. [PubMed: 27959613]

Fry DW, Harvey PJ, Keller PR, Elliott WL, Meade M, Trachet E, Albassam M, Zheng X, Leopold WR, Pryer NK, and Toogood PL (2004). Specific inhibition of cyclin-dependent kinase 4/6 by PD 0332991 and associated antitumor activity in human tumor xenografts. Mol Cancer Ther 3, 1427–1438. [PubMed: 15542782]

Futreal PA, Coin L, Marshall M, Down T, Hubbard T, Wooster R, Rahman N, and Stratton MR (2004). A census of human cancer genes. Nat Rev Cancer 4, 177–183. [PubMed: 14993899]

Hortobagyi GN, Stemmer SM, Burris HA, Yap YS, Sonke GS, Paluch-Shimon S, Campone M, Blackwell KL, Andre F, Winer EP, et al. (2016). Ribociclib as First-Line Therapy for HR-Positive, Advanced Breast Cancer. N Engl J Med 375, 1738–1748. [PubMed: 27717303]

Jeselsohn R, Yelensky R, Buchwalter G, Frampton G, Meric-Bernstam F, Gonzalez-Angulo AM, Ferrer-Lozano J, Perez-Fidalgo JA, Cristofanilli M, Gomez H, et al. (2014). Emergence of constitutively active estrogen receptor-alpha mutations in pretreated advanced estrogen receptor-positive breast cancer. Clin Cancer Res 20, 1757–1767. [PubMed: 24398047]

Johnston S, Pippen J, Jr., Pivot X, Lichinitser M, Sadeghi S, Dieras V, Gomez HL, Romieu G, Manikhas A, Kennedy MJ, et al. (2009). Lapatinib combined with letrozole versus letrozole and placebo as first-line therapy for postmenopausal hormone receptor-positive metastatic breast cancer. J Clin Oncol 27, 5538–5546. [PubMed: 19786658]

Kandoth C, McLellan MD, Vandin F, Ye K, Niu B, Lu C, Xie M, Zhang Q, McMichael JF, Wyczalkowski MA, et al. (2013). Mutational landscape and significance across 12 major cancer types. Nature 502, 333–339. [PubMed: 24132290]

Lawrence MS, Stojanov P, Mermel CH, Robinson JT, Garraway LA, Golub TR, Meyerson M, Gabriel SB, Lander ES, and Getz G (2014). Discovery and saturation analysis of cancer genes across 21 tumour types. Nature 505, 495–501. [PubMed: 24390350]

Li Q, Wang H, Zogopoulos G, Shao Q, Dong K, Lv F, Nwilati K, Gui XY, Cuggia A, Liu JL, and Gao ZH (2016). Reg proteins promote acinar-to-ductal metaplasia and act as novel diagnostic and prognostic markers in pancreatic ductal adenocarcinoma. Oncotarget 7, 77838–77853. [PubMed: 27788482]

Liao Y, Smyth GK, and Shi W (2013). The Subread aligner: fast, accurate and scalable read mapping by seed-and-vote. Nucleic Acids Res 41, e108. [PubMed: 23558742]

Liao Y, Smyth GK, and Shi W (2014). featureCounts: an efficient general purpose program for assigning sequence reads to genomic features. Bioinformatics 30, 923–930. [PubMed: 24227677]

Love MI, Huber W, and Anders S (2014). Moderated estimation of fold change and dispersion for RNA-seq data with DESeq2. Genome Biol 15, 550. [PubMed: 25516281]

Martelotto LG, Ng CK, De Filippo MR, Zhang Y, Piscuoglio S, Lim RS, Shen R, Norton L, Reis-Filho JS, and Weigelt B (2014). Benchmarking mutation effect prediction algorithms using functionally validated cancer-related missense mutations. Genome Biol 15, 484. [PubMed: 25348012]

Martin D, Degese MS, Vitale-Cross L, Iglesias-Bartolome R, Valera JLC, Wang Z, Feng X, Yeerna H, Vadmal V, Moroishi T, et al. (2018). Assembly and activation of the Hippo signalome by FAT1 tumor suppressor. Nat Commun 9, 2372. [PubMed: 29985391]

Matsushime H, Ewen ME, Strom DK, Kato JY, Hanks SK, Roussel MF, and Sherr CJ (1992). Identification and properties of an atypical catalytic subunit (p34PSK-J3/cdk4) for mammalian D type G1 cyclins. Cell 71, 323–334. [PubMed: 1423597]

Morris LG, Kaufman AM, Gong Y, Ramaswami D, Walsh LA, Turcan S, Eng S, Kannan K, Zou Y, Peng L, et al. (2013). Recurrent somatic mutation of FAT1 in multiple human cancers leads to aberrant Wnt activation. Nat Genet 45, 253–261. [PubMed: 23354438]

O'Leary B, Cutts RJ, Liu Y, Hrebien S, Huang X, Fenwick K, Andre F, Loibl S, Loi S, Garcia-Murillas I, et al. (2018). The genetic landscape and clonal evolution of breast cancer resistance to palbociclib plus fulvestrant in the PALOMA-3 trial. Cancer Discov.

Polak P, Kim J, Braunstein LZ, Karlic R, Haradhavala NJ, Tiao G, Rosebrock D, Livitz D, Kubler K, Mouw KW, et al. (2017). A mutational signature reveals alterations underlying deficient homologous recombination repair in breast cancer. Nat Genet 49, 1476–1486. [PubMed: 28825726]

Razavi P, Chang MT, Xu G, Bandlamudi C, Ross DS, Vasan N, Cai Y, Bielski CM, Donoghue MTA, Jonsson P, et al. (2018). The Genomic Landscape of Endocrine-Resistant Advanced Breast Cancers. Cancer Cell 34, 427–438 e426. [PubMed: 30205045]

Riaz N, Blecua P, Lim RS, Shen R, Higginson DS, Weinhold N, Norton L, Weigelt B, Powell SN, and Reis-Filho JS (2017). Pan-cancer analysis of bi-allelic alterations in homologous recombination DNA repair genes. Nat Commun 8, 857. [PubMed: 29021619]

Robinson DR, Wu YM, Vats P, Su F, Lonigro RJ, Cao X, Kalyana-Sundaram S, Wang R, Ning Y, Hodges L, et al. (2013). Activating ESR1 mutations in hormone-resistant metastatic breast cancer. Nat Genet 45, 1446–1451. [PubMed: 24185510]

Sanchez-Vega F, Mina M, Armenia J, Chatila WK, Luna A, La KC, Dimitriadoy S, Liu DL, Kantheti HS, Saghafinia S, et al. (2018). Oncogenic Signaling Pathways in The Cancer Genome Atlas. Cell 173, 321–337 e310. [PubMed: 29625050]

Sanjana NE, Shalem O, and Zhang F (2014). Improved vectors and genome-wide libraries for CRISPR screening. Nat Methods 11, 783–784. [PubMed: 25075903]

Schwarz JM, Rodelsperger C, Schuelke M, and Seelow D (2010). MutationTaster evaluates disease-causing potential of sequence alterations. Nat Methods 7, 575–576. [PubMed: 20676075]

Shalem O, Sanjana NE, Hartenian E, Shi X, Scott DA, Mikkelson T, Heckl D, Ebert BL, Root DE, Doench JG, and Zhang F (2014). Genome-scale CRISPR-Cas9 knockout screening in human cells. Science 343, 84–87. [PubMed: 24336571]

Shen R, and Seshan VE (2016). FACETS: allele-specific copy number and clonal heterogeneity analysis tool for high-throughput DNA sequencing. Nucleic Acids Res 44, e131. [PubMed: 27270079]

Shihab HA, Gough J, Cooper DN, Stenson PD, Barker GL, Edwards KJ, Day IN, and Gaunt TR (2013). Predicting the functional, molecular, and phenotypic consequences of amino acid substitutions using hidden Markov models. Hum Mutat 34, 57–65. [PubMed: 23033316]

Silva E, Tsatskis Y, Gardano L, Tapon N, and McNeill H (2006). The tumor-suppressor gene fat controls tissue growth upstream of expanded in the hippo signaling pathway. Curr Biol 16, 2081–2089. [PubMed: 16996266]

Skouloudaki K, Puetz M, Simons M, Courbard JR, Boehlke C, Hartleben B, Engel C, Moeller MJ, Englert C, Bollig F, et al. (2009). Scribble participates in Hippo signaling and is required for normal zebrafish pronephros development. Proc Natl Acad Sci U S A 106, 85798584.

Sledge GW, Jr., Toi M, Neven P, Sohn J, Inoue K, Pivot X, Burdaeva O, Okera M, Masuda N, Kaufman PA, et al. (2017). MONARCH 2: Abemaciclib in Combination With Fulvestrant in Women With HR+/HER2- Advanced Breast Cancer Who Had Progressed While Receiving Endocrine Therapy. J Clin Oncol 35, 2875–2884. [PubMed: 28580882]

Subramanian A, Tamayo P, Mootha VK, Mukherjee S, Ebert BL, Gillette MA, Paulovich A, Pomeroy SL, Golub TR, Lander ES, and Mesirov JP (2005). Gene set enrichment analysis: a knowledge-based approach for interpreting genome-wide expression profiles. Proc Natl Acad Sci U S A 102, 15545–15550. [PubMed: 16199517]

Toy W, Shen Y, Won H, Green B, Sakr RA, Will M, Li Z, Gala K, Fanning S, King TA, et al. (2013). ESR1 ligand-binding domain mutations in hormone-resistant breast cancer. Nat Genet 45, 1439–1445. [PubMed: 24185512]

Turner NC, Ro J, Andre F, Loi S, Verma S, Iwata H, Harbeck N, Loibl S, Huang Bartlett C, Zhang K, et al. (2015). Palbociclib in Hormone-Receptor-Positive Advanced Breast Cancer. N Engl J Med 373, 209–219. [PubMed: 26030518]

Tyler DM, and Baker NE (2007). Expanded and fat regulate growth and differentiation in the Drosophila eye through multiple signaling pathways. Dev Biol 305, 187–201. [PubMed: 17359963]

Willecke M, Hamaratoglu F, Kango-Singh M, Udan R, Chen CL, Tao C, Zhang X, and Halder G (2006). The fat cadherin acts through the hippo tumor-suppressor pathway to regulate tissue size. Curr Biol 16, 2090–2100. [PubMed: 16996265]

Xie Q, Chen J, Feng H, Peng S, Adams U, Bai Y, Huang L, Li J, Huang J, Meng S, and Yuan Z (2013). YAP/TEAD-mediated transcription controls cellular senescence. Cancer Res 73, 3615–3624. [PubMed: 23576552]

Yang C, Li Z, Bhatt T, Dickler M, Giri D, Scaltriti M, Baselga J, Rosen N, and Chandarlapaty S (2017). Acquired CDK6 amplification promotes breast cancer resistance to CDK4/6 inhibitors and loss of ER signaling and dependence. Oncogene 36, 2255–2264. [PubMed: 27748766]

Yates LR, Knappskog S, Wedge D, Farmery JHR, Gonzalez S, Martincorena I, Alexandrov LB, Van Loo P, Haugland HK, Lilleng PK, et al. (2017). Genomic Evolution of Breast Cancer Metastasis and Relapse. Cancer Cell 32, 169–184 e167. [PubMed: 28810143]

Zehir A, Benayed R, Shah RH, Syed A, Middha S, Kim HR, Srinivasan P, Gao J, Chakravarty D, Devlin SM, et al. (2017). Mutational landscape of metastatic cancer revealed from prospective clinical sequencing of 10,000 patients. Nat Med 23, 703–713. [PubMed: 28481359]

SIGNIFICANCE

CDK4/6 inhibitors have proven effective in treating ER^+ breast cancer and have shown promising activity against several other cancers. However, resistance to CDK4/6 inhibitors is often found and not well understood. Here we identified upregulation of CDK6 kinase as a recurrent mechanism of resistance. We specifically find loss of the *FAT1* tumor suppressor, a gene mutated in many cancers, to promote clinical resistance and cause increased CDK6 expression. FAT1 is demonstrated to regulate CDK6 via the Hippo signaling pathway. These findings identify a critical role for the Hippo pathway in cell cycle regulation and drug resistance and suggest a potential benefit for more potent inhibitors of CDK6 kinase as strategies to circumvent resistance.

FAT1 or *RB1* loss is associated with clinical resistance to CDK4/6 inhibitors

Knockout of *FAT1* causes Hippo pathway suppression in ER^+ cancers

YAP/TAZ nuclear localization induces CDK6 overexpression

Genomic alterations causing YAP activation lead to CDK6-mediated resistance

Li et al. identify inactivation of RB1 and FAT1 to be associated with resistance of ER^+ breast cancer to CDK4/6 inhibitors (CDK4/6i). FAT1 loss increases CDK6 expression via the Hippo pathway. Inactivation of the Hippo pathway component NF2 also increases CDK6 expression and reduces sensitivity to CDK4/6i.

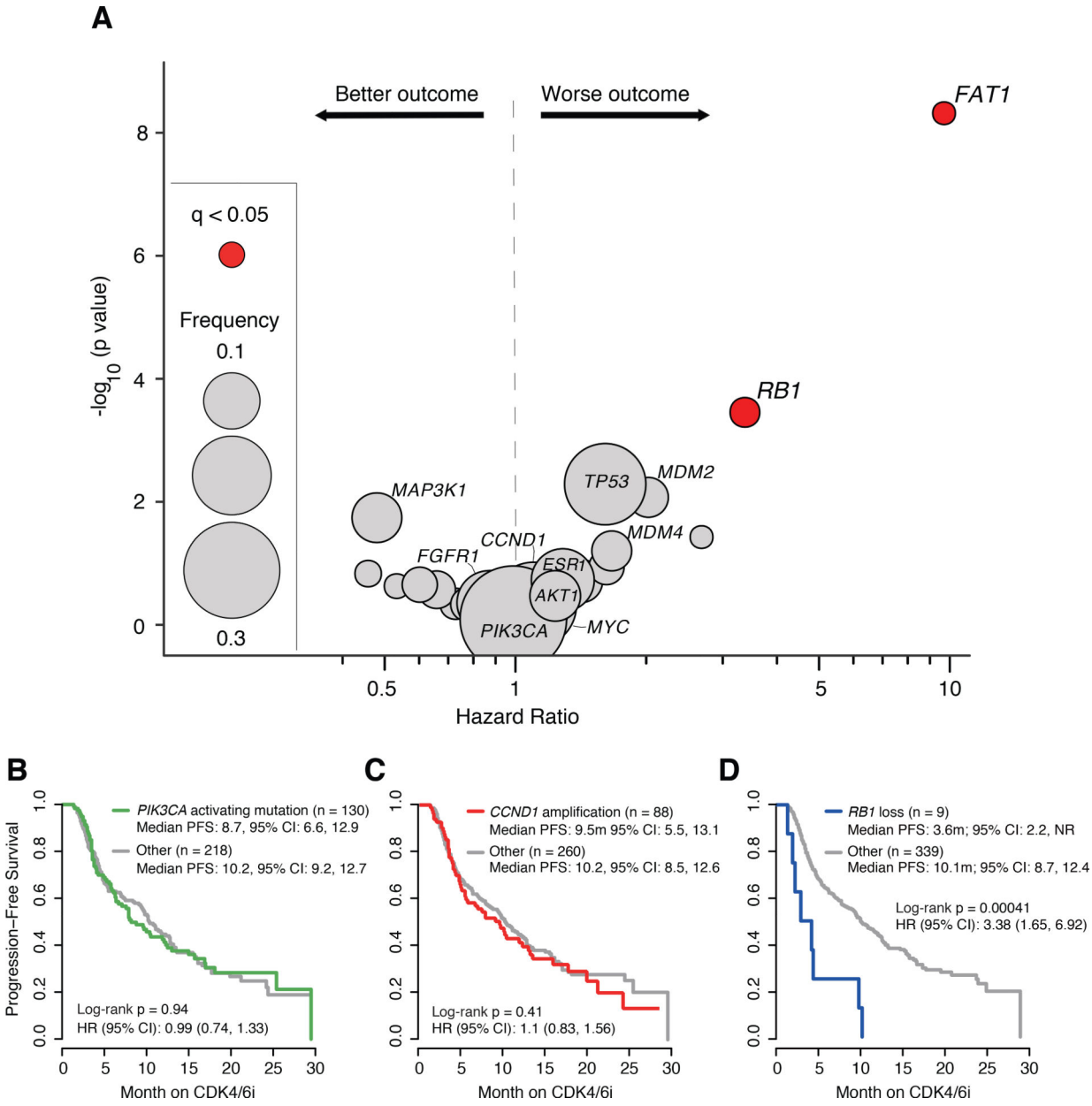

Figure 1. Genomic alterations correlated with CDK4/6 inhibitor resistance.

(**A**) The significance of association of altered genes with progression-free survival (PFS) on CDK4/6i based on Cox proportional hazard models. Color indicates statistical significance by (q value < 0.05) and size of the circle reflects the frequency of alteration in the cohort. All q values are calculated based on Benjamini and Hochberg method correction of log-rank p values. (**B, C, D**) PFS of patients receiving CDK4/6i and with tumors harboring functional alterations in *PIK3CA* (**B**), *CCND1* amplification (**C**), and *RB1* loss (**D**) as compared to patients whose tumors were wild-type for these lesions (gray). Hazard ratios (HR) and 95% confidence intervals (95% CI) are based on Cox proportional hazard models stratified by regimen. All p values as indicated, log-rank test.

See also Figure S1 and Tables S1-S4.

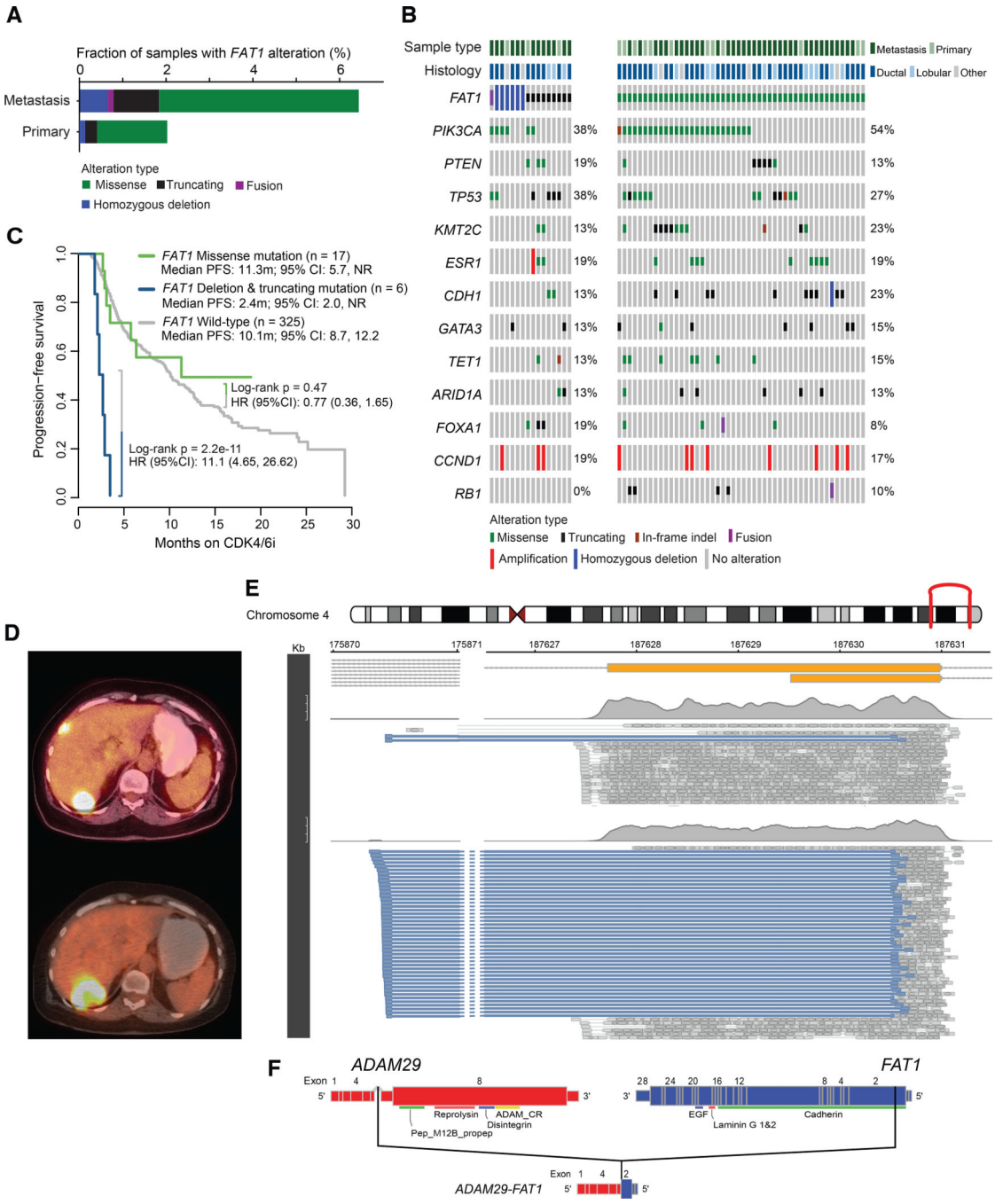

Figure 2. *FAT1* loss and clinical resistance.

(**A**) Frequency of type of *FAT1* alterations by type of tumor sample (metastatic vs primary) in 1501 ER$^+$ breast cancer cases (**B**) The pattern, frequency, and type of genomic alterations in key breast cancer genes of the tumors presented in panel A by different classes of *FAT1* alterations, comparing the *FAT1* homozygous deletion or truncating mutations (left) with *FAT1* missense mutations (right). (**C**) progression-free survival (PFS) of patients receiving CDK4/6i with tumors harboring *FAT1* missense mutations (green), homozygous deletion or truncating mutations (blue) as compared to patients whose tumors were wild-type for these

lesions (gray). Hazard ratios (HR) and 95% confidence intervals (95% CI) are based on Cox proportional hazard models stratified by regimen. All p values as indicated, log-rank test. (**D**) Baseline and post-progression PET-CT scan of the liver lesion in a patient (PFS 2.5 months) on palbociclib and fulvestrant. (**E**) Alignments of sequence reads on chromosome 4 in the pre-treatment lung lesion (top) and post-treatment liver lesion (bottom) showing paired ends encompassing the chr4:175870481–187630480 deletion (blue) along with sequence reads having close to average insert size (grey). The deletion is represented schematically by the red connected vertical lines on the chromosome ideogram. In the intermediate panels, the orange and grey bars display all the transcripts predicted for *ADAM29* and *FAT1* in Ensembl while the corresponding grey density plots above each sequence alignment window show the base level coverage (scale on the y-axis to the left). The *ADAM29-FAT1* fusion was detected in the post-treatment liver tumor (bottom, supported by 46 paired-reads, average depth of coverage 791x) but was not called in the pre-treatment lung tumor (detected 2 paired-reads, average depth of coverage 1309x). In all panels, genomic coordinates are Kb as displayed immediately below the chromosome ideogram. (**F**) Schematic representation of the *ADAM29-FAT1* fusion inferred from the mapping positions to the paired ends and based on the Ensembl canonical transcripts of the two genes.

See also Figure S2 and Tables S1-S3.

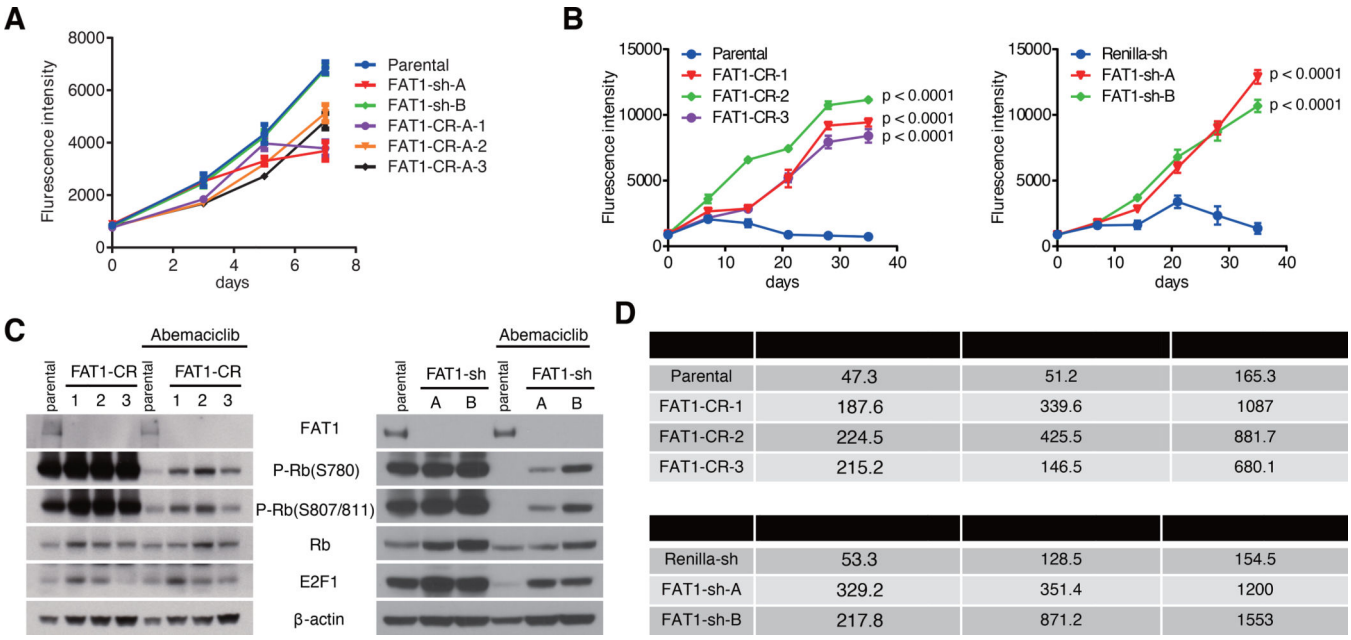

Parental	47.3	51.2	165.3
FAT1-CR-1	187.6	339.6	1087
FAT1-CR-2	224.5	425.5	881.7
FAT1-CR-3	215.2	146.5	680.1

Renilla-sh	53.3	128.5	154.5
FAT1-sh-A	329.2	351.4	1200
FAT1-sh-B	217.8	871.2	1553

Figure 3. FAT1 loss promotes resistance to CDK4/6 inhibitors.

(**A**) Proliferation of FAT1-sh, FAT1-CR, and parental MCF7 cells without drug treatment. Data are represented as mean ± SD; n = 3. (**B**) Proliferation of *FAT1*-loss and parental MCF7 cells exposed to 50 nM of abemaciclib. Data are represented as mean ± SD; n = 3. All p values are based on one-way ANOVA test of day 35 data with Dunnett's method correction compared with parental. (**C**) Immunoblotting of total and phosphorylated Rb in parental and *FAT1*-loss cells. (**D**) IC_{50}s of abemaciclib, palbociclib or ribociclib in different MCF7 cell models. IC_{50}s were calculated based on day 5 data of various doses of drug treatment.

See also Figure S3.

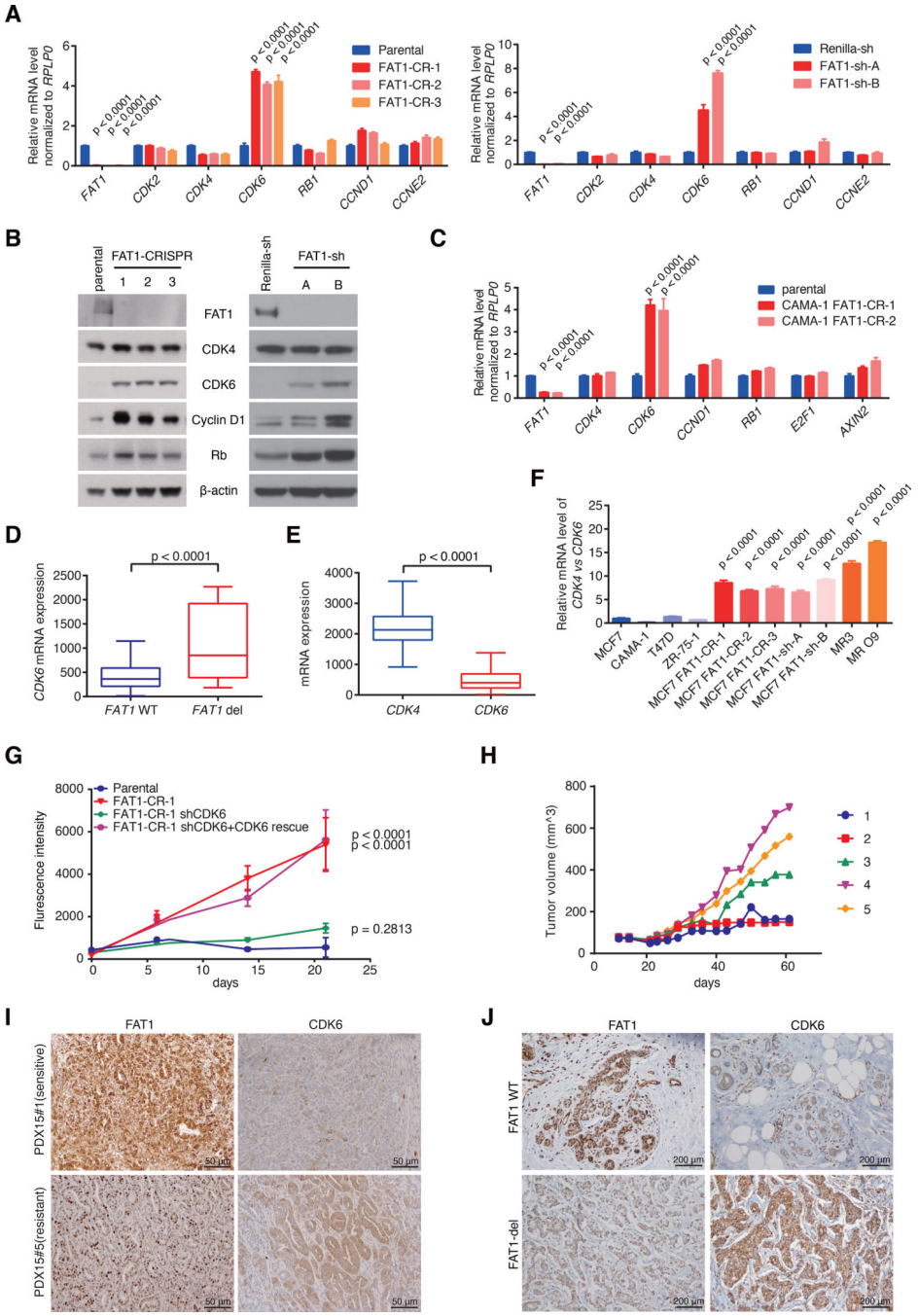

Figure 4. FAT1 suppresses CDK6 expression.

(**A**) Relative mRNA level of indicated genes normalized to *RPLP0* in FAT1-CR, FAT1-sh, Renilla-sh, and parental MCF7 cells. Data are represented as mean ± SD; n = 3. All p values are based on one-way ANOVA test with Dunnett's method correction compared with parental or Renilla-sh. (**B**) Immunoblotting of CDK4/6 and cyclin D in parental and *FAT1*-loss MCF7 cells.

(**C**) Relative mRNA level of indicated genes normalized to *RPLP0* in FAT1-CR and parental CAMA-1 cell. Data are represented as mean ± SD; n = 3. All p values are based on one-way

ANOVA test with Dunnett's method correction compared with parental. (**D**) mRNA expression of *CDK6* in the cohort of patients with ER^+ breast cancer (TCGA provisional dataset) harboring *FAT1* wild-type or deletion alteration was analyzed and p values were calculated using two-tailed Student's t-tests. (**E**) mRNA expression of *CDK4* and *CDK6* in the cohort of patients with ER^+ breast cancer (TCGA provisional dataset) was analyzed and p values were calculated using two-tailed Student's t-tests. For (D) and (E), the bottom and top of the boxplot represent the lower and upper quartiles, respectively, and the band near the middle of the box represents the median. The upper whisker represents the upper quartile + 1.5 x interquartile range (IQR) and the lower whisker represents the lower quartile - 1.5 x IQR. (**F**) Ratio of mRNA expression of *CDK6* normalized to that of *CDK4* in multiple CDK4/6i-resistant (red/orange) and sensitive (blue) ER^+ breast cancer models. Data are represented as mean ± SD; n = 3. All p values are based on one-way ANOVA test with Dunnett's method correction compared with MCF7. (**G**) Proliferation of parental and FAT1-CR-1 cells, constitutively expressing CDK6-shRNA, or CDK6shRNA plus CDK6 re-expression, exposed to 100 nM of abemaciclib. Data are represented as mean ± SD; n = 3. All p values are based on one-way ANOVA test with Dunnett's method correction compared with parental. (**H**) Tumor growth curve of PDXs in response to ribociclib treatment (200 mg/kg). (**I**) Representative immunohistochemical (IHC) images of PDX samples with different sensitivity to CDK4/6 inhibitors stained with FAT1 or CDK6 antibodies. Scale bars 50 μm. (**J**) Representative IHC images of human breast tumors with different FAT1 alterations stained with FAT1 or CDK6 antibodies. Scale bars 200 μm.
See also Figure S4.

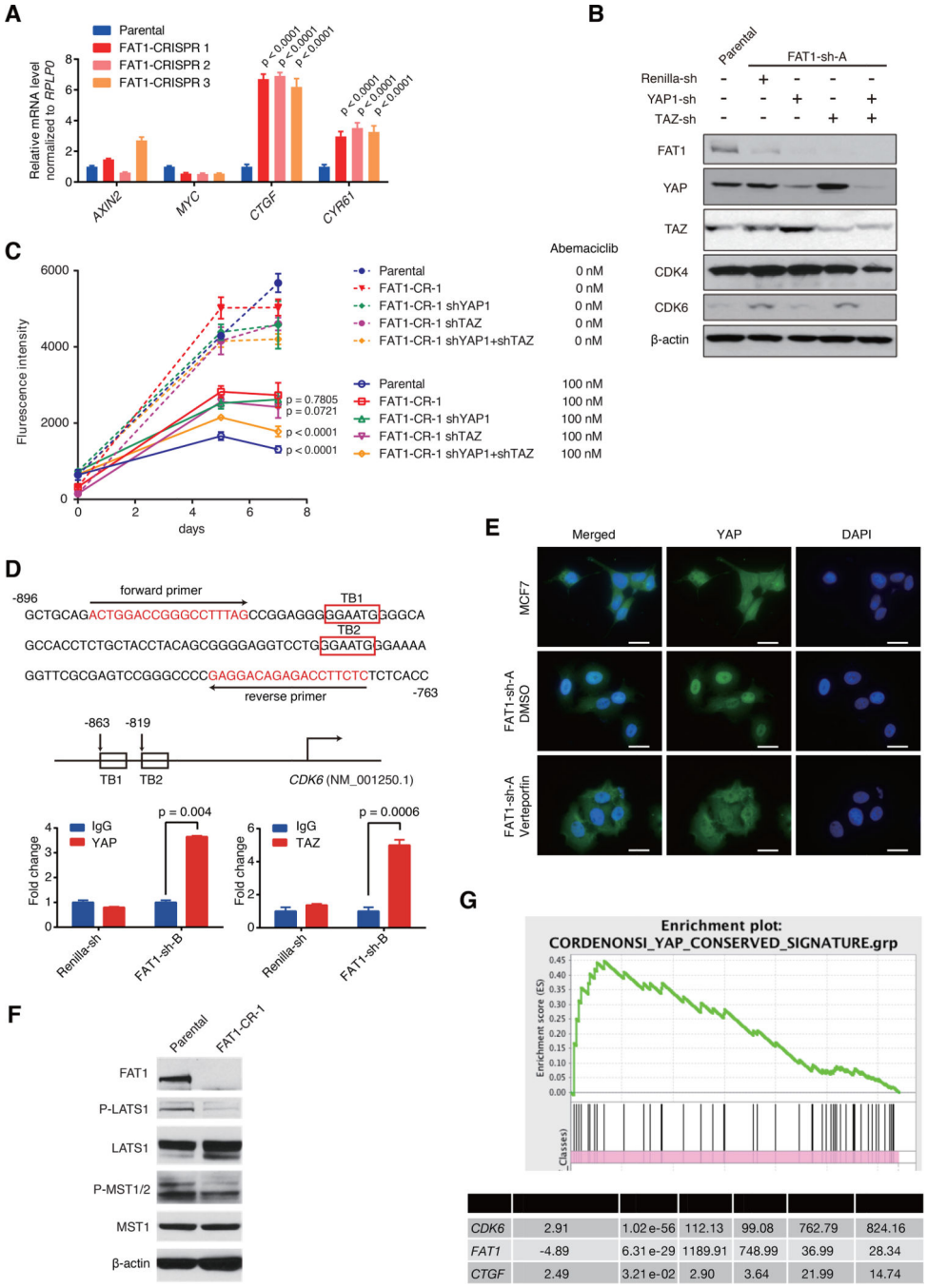

CDK6	2.91	1.02 e-56	112.13	99.08	762.79	824.16
FAT1	-4.89	6.31 e-29	1189.91	748.99	36.99	28.34
CTGF	2.49	3.21 e-02	2.90	3.64	21.99	14.74

Figure 5. CDK6 is regulated by Hippo signaling in ER$^+$ breast cancer cells

(A) Relative mRNA expression of indicated genes normalized to *RPLP0* in FAT1-CR and parental MCF7 cells. Data are represented as mean ± SD; n = 3. All p values are based on one-way ANOVA statistical test with Dunnett's method correction compared with parental. (B) Immunoblotting of indicated proteins in parental and FAT1 ablation cells with YAP1 and/or TAZ knockdown. (C) Proliferation of parental and FAT1-CR-1 cells, constitutively expressing YAP1-shRNA and/or TAZ-shRNA, with or without 100 nM of abemaciclib treatment. Data are represented as mean ± SD; n = 3. All p values are based on one-way

ANOVA test with Dunnett's method correction compared with FAT1-CR-1. (D) ChIP-qPCR assay for YAP/TAZ showing induction of binding to CDK6 promoter upon FAT1 knockdown. Data are represented as mean ± SD; n = 3. All p values are based on two-tailed Student's t-tests. (E) Immunofluorescent images of YAP (green) localization in parental MCF7 and FAT-sh-A cells treated with DMSO or 10 μM verteporfin. DAPI included as a nuclear stain (blue). Scale bars, 20 μm. (F) Phosphorylation and expression of Hippo pathway components in parental and FAT1 ablation MCF7 cells. (G) Gene enrichment analysis of RNA-seq result using GSEA. The relative expression of *FAT1*, *CDK6* and *CTGF* in RNA-seq is summarized at the bottom.

See also Figure S5 and Table S5.

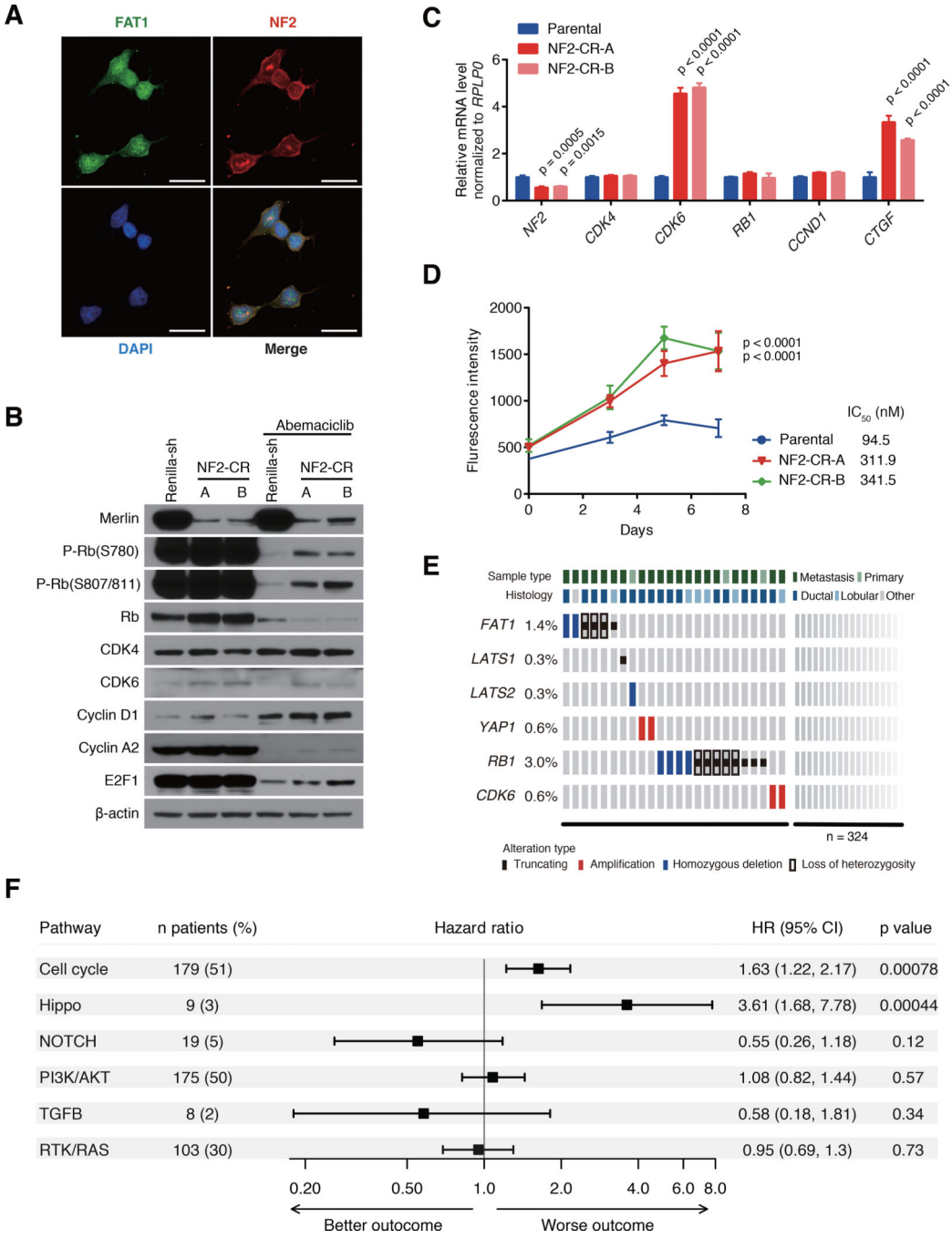

Figure 6. Genomic alterations in the Hippo signaling pathway and CDK4/6i resistance.

(**A**) Immunofluorescence images for FAT1 (green) and NF2 (red) in MCF7 cells. DAPI was used as a nuclear stain (blue). Scale bars, 20 μm. (**B**) Immunoblotting for cyclin D-CDK4/6 and Rb in parental and *NF2* knockout (NF2-CR) MCF7 cells in the absence or presence of 100 nM abemaciclib. (**C**) Relative mRNA expression of indicated genes normalized to that of *RPLP0* in NF2-CR and parental MCF7 cells. Data are represented as mean ± SD; n = 3. All p values are based on one-way ANOVA test with Dunnett's method correction compared with parental. (**D**) Proliferation of NF2-CR and parental MCF7 cells in the presence of 50

nM abemaciclib. Data are represented as mean ± SD; n = 3. All p values one-way ANOVA statistical test of day 5 data with Dunnett's method correction compared with parental. (**E**) Pattern and frequency of likely pathogenic mutations and focal amplifications or deletions targeting components of the Hippo pathway including *FAT1*, *LATS1*, *LATS2*, and *YAP1* and Cell Cycle pathway including *RB1*, and *CDK6*. (**F**) Association of altered pathways with PFS on CDK4/6i. Hazard ratios (HR) and 95% confidence intervals (9% CI) are based on Cox proportional hazard models stratified by regimen. Error bars represent 95% CIs.
See also Table S6.